

Eurocode 8-compatible synthetic time-series as input to dynamic analysis

Mathieu Causse, Aurore Laurendeau, Mathieu Perrault, John Douglas, Luis Fabian Bonilla, Philippe Guéguen

▶ **To cite this version:**

Mathieu Causse, Aurore Laurendeau, Mathieu Perrault, John Douglas, Luis Fabian Bonilla, et al.. Eurocode 8-compatible synthetic time-series as input to dynamic analysis. Bulletin of Earthquake Engineering, 2014, 12 (2), pp.755-768. 10.1007/s10518-013-9544-2 . hal-00878538

HAL Id: hal-00878538
https://brgm.hal.science/hal-00878538

Submitted on 30 Oct 2013

HAL is a multi-disciplinary open access archive for the deposit and dissemination of scientific research documents, whether they are published or not. The documents may come from teaching and research institutions in France or abroad, or from public or private research centers.

L'archive ouverte pluridisciplinaire **HAL**, est destinée au dépôt et à la diffusion de documents scientifiques de niveau recherche, publiés ou non, émanant des établissements d'enseignement et de recherche français ou étrangers, des laboratoires publics ou privés.

Eurocode 8-compatible synthetic time-series as input to dynamic analysis

M. Causse[1], A. Laurendeau[1], M. Perrault[1], J. Douglas[3], L.F. Bonilla[2], P. Guéguen[1]

1: ISTerre, CNRS, Université Joseph Fourier, IFFSTAR, Grenoble, France

2: Université Paris Est - IFSTTAR, Paris, France

3: BRGM – DRP/RSV, Orléans, France

Corresponding author:

Mathieu Causse

ISTerre – BP 53

38041 Grenoble cedex 9

mathieu.causse@ujf-grenoble.fr

Phone : 0033476635173

ABSTRACT:

Nonlinear dynamic analysis of existing or planned structures often requires the use of accelerograms that match a target design spectrum. Here, our main concern is to generate a set of motions with a good level of fit to the Eurocode 8 (EC8) design spectra for France. Synthetic time series are generated by means of a non-stationary stochastic method. To calibrate the input parameters in the stochastic approach, we select a reference set of accelerograms for a Eurocode 8 type B site category from the PEER Ground-Motion Database, which are then adjusted to the target spectrum through wavelet addition. Then, we compute nonlinear seismic responses of a soil column, including pore pressure effects, and brittle and ductile structures to the stochastic time-series, the natural accelerograms and time-series generated using stationary stochastic approaches. The results of these calculations

reveal considerable variability in response despite the similarities in terms of spectral acceleration.

Keywords: Eurocode 8 (EC8), spectrum-compatible time-series, nonlinear site response, structural response, variability

1. INTRODUCTION

The selection of accelerograms for earthquake engineering (both geotechnical and structural branches) is becoming increasingly important with the growing use of nonlinear dynamic analysis, for which a set of input ground motions is a key component. Sets of accelerograms can be obtained/generated in various ways, including purely natural accelerograms (e.g. Bommer and Acevedo 2004) through to purely artificial (e.g. Gasparini and Vanmarcke 1979) via various types in between (e.g. Douglas and Aochi, 2008). Whatever the technique deployed, it is necessary that the input ground motions be compatible with the assumed earthquake scenario, usually described in terms of a magnitude-distance pair (and possibly other descriptors, e.g. focal mechanism, and number of standard deviations from the mean), level of ground-motion intensity and/or design response spectrum. This condition sometimes implies that input motions are adjusted: often simply by linear scaling, by adding harmonic components in the frequency domain (e.g., using WES RASCAL, Silva and Lee, 1987) or by wavelet adjustments to obtain spectrum-compatible accelerograms (e.g., using RSPMatch, Abrahamson, 1992; Hancock et al. 2006). It is vital that the set of motions allows the accurate prediction of the average response of the analyzed system but also an indication of the variability around this average due to possibly variations in ground motions (e.g. Douglas, 2006).

Various recent studies attempt to define criteria to select sets of accelerograms suitable

for dynamic analyses. Özer and Akkar (2012) propose a strategy to select and scale earthquake records that provides good estimates of the median response and variability of nonlinear structural systems without excessively changing the inherent features of the selecting recordings. Buratti et al. (2011) present criteria to select six time-series (two original records, each scaled to three target levels), which they use to obtain a reasonable estimate of the full distribution of drift response in a six-story reinforced-concrete (RC) frame building. In dynamic analyses, a crucial step is the selection of accelerograms with appropriate spectral shapes, a condition that cannot be achieved in case of excessive scaling (Watson-Lamprey and Abrahamson 2006). To ensure realistic spectral shapes (e.g. in agreement with a given magnitude-distance scenario), Rota et al. (2012) propose a method to find a suite of accelerograms compatible with the Italian design spectra at any location in Italy. They derive a seismic mesozonation of the Italian territory, based on the identification of groups of spectra with similar features. For each of these groups, a reference spectrum is defined and then used to select real spectrum-compatible records.

However, natural records corresponding to the earthquake scenario and site condition of the target spectrum are not always available. In this case simulations are needed. Among the available simulations techniques, stochastic simulations are widely used because of their simplicity. As summarized by Douglas and Aochi (2008), there are various types of stochastic methods: stationary stochastic methods that are compatible with a target spectrum (e.g., SIMQKE, Gasparini and Vanmarcke, 1976), semi-empirical methods taking into account non-stationarity that are compatible with a target spectrum (e.g., Rezaeian and Der Kiureghian, 2010) and methods incorporating earthquake physics (e.g., Pousse et al. 2006).

Some recent studies compare the impact of using different techniques on the results of the final engineering analysis. Schwab and Lestuzzi (2007) carried out nonlinear analyses on single-degree-of-freedom (SDOF) systems using time-series produced by the classic

stochastic stationary procedure of SIMQKE (Gasparini and Vanmarcke 1976) as well as semi-empirical non-stationary stochastic simulations (Sabetta and Pugliese, 1996). They show that the classic stationary procedure leads to a significant underestimation of the ductility demand compared to natural accelerograms, whereas the non-stationary procedure performs much better. Iervolino et al. (2010a) examine the mean nonlinear response of SDOF systems in terms of demand spectra (peak and cyclic response) using various sets of accelerograms, both real and artificial. They found that artificial records tend to underestimate the peak demand and to overestimate cyclic response. They do not give any conclusions on the variability of the response of the SDOF system. Along this line, Atkinson and Goda (2010) investigate peak nonlinear response of SDOF systems subjected to physics-based extended stochastic simulations (EXSIM software, Motazedian and Atkinson 2005) and lightly modified and scaled real records. They suggest that the stochastic method may be able to capture the overall structure response. But again, they do not address response variability.

Recently, Sextos et al. (2011) chose an existing building damaged by the 2003 Lefkada earthquake as a case study. Taking advantage of the availability of the ground-motion excitation and damage observation, they calibrated a finite-element model of the building using the observed response and conducted extensive parametric analyses for various EC8-compliant sets of real accelerograms. They show that the main conclusions on the effects of the accelerogram selection on SDOF non-linear systems remain valid for more realistic irregular buildings. They also claim that EC8 specifications are too restrictive when selecting appropriate sets of accelerograms for reliable dynamic analysis.

Given the little guidance provided in the EC8 design code on how to select/generate code-compatible time-series a number of recent articles have proposed sets of accelerograms consistent with the standard EC8 spectra. Kayhan et al. (2011) develop a meta-heuristic harmony search algorithm to select and linearly-scale sets of seven natural accelerograms

from the PEER Ground-Motion Database whose average spectra match the EC8 spectrum for the five principal EC8 site classes. Iervolino et al. (2010b) present a software package (REXEL) that allows suites of natural accelerograms to be selected from online European strong-motion databases whose averages match the EC8 spectral shape. Various options to adjust the selection algorithm (e.g. magnitude-distance ranges) are provided to the user. As mentioned above, Rota et al. (2012) also propose a method and suites of accelerograms for use in EC8-based design and analysis for Italy. These three studies are based on selection and scaling of natural strong-motion records. In contrast, Giaralis and Spanos (2009) propose a wavelet-based technique to generate artificial spectrum-compatible accelerograms, which they then apply to produce suites of EC8-compatible records.

The current article differs from these previous studies in three main ways. Firstly, previous studies are all based on the standard EC8 spectra, whereas the present study focuses on the Type 2 EC8 spectrum in application in France. This spectrum differs not only from the standard Type 1 shape, but also from the standard Type 2 spectrum at long periods [see Figure 1 and Pousse et al. (2005)]. Secondly, these previous studies concentrated on providing accelerograms whose averages match code spectra rather than also explicitly seeking suites whose variability matches the true dispersion in earthquake ground motions. Thirdly, the additional step of using the proposed time-series as inputs to structural and/or geotechnical analyses was rarely made. This is an important step because it allows the variability in the response of engineering systems due to differences in the input ground motions (all of which are compatible with the code) to be assessed.

2. TIME-SERIES

As a common basis for this study we queried the PEER Ground-Motion Database (http://peer.berkeley.edu/peer_ground_motion_database/spectras/new) to find ten

accelerograms with $5.8 \leq M_w \leq 6.2$, $0 \leq r_{rup} \leq 20$km (where r_{rup} is the distance to the rupture) and $400 \leq V_{s30} \leq 600$m/s that best match the French version of the EC8 design spectrum for a class B site (see Table 1). This database provides free access to thousands of strong-motion records from shallow crustal earthquakes in active areas and also easy-to-use online tools for the selection of records that match criteria in terms of earthquake scenario, local site conditions and response spectra. To not underestimate the true variability in ground motions or to bias the results by site- or event-specific characteristics we did not select more than one record from a given earthquake or a given site. For each triaxial accelerogram, the single component that best matched the EC8 spectrum from the two horizontal components was selected and scaled to a target peak ground acceleration (PGA) of 0.22g (the design PGA for a class B site in the highest hazard areas of mainland France). This set of accelerograms is the first set of input motions and it is called here: *Natural_Scaled*. There is a large variability in the response spectra of these signals even though, on average, they match the target spectrum quite well.

These ten accelerograms were then adjusted in the period range 0.1 – 1s using the software SeismoMatch (http://www.seismosoft.com/en/HomePage.aspx), which adds wavelets so that the response spectra more closely match the target without greatly changing the "look" of the accelerograms. After applying this spectral matching the response spectra show a much closer match to the target spectrum, although they still lack short-period energy, but the accelerograms retain much variability in the time-domain. This is the second set of input motions and it is called here: *Natural_Matched*.

Until recently, many engineering studies used SIMQKE (Gasparini and Vanmarcke, 1976) to create accelerograms whose response spectra match a target. Although this technique is no longer considered state-of-the-art, we generate ten accelerograms to match the target EC8 spectrum using SIMQKE as a test of the validity of such an approach. So that the durations of the SIMQKE accelerograms are physically realistic we adopted the exponential

envelope function with *a* and *b* parameters that led to a relative significant duration (5-95% of Arias intensity) close to the median duration predicted by the ground-motion prediction equation of Abrahamson & Silva (1996) for M_w=6 at r_{rup}=10km and V_{s30}=500m/s (7.7s). These accelerograms have spectra that exactly match the target and there are all very similar in the time-domain. This is the third set of input motions and it is called here: *SIMQKE*.

In the original SIMQKE procedure, a white-noise time series is filtered with an exponential envelope in the time domain. The phase of the output time histories is chosen randomly. In this study, we use a modified version by using natural phase accelerograms to obtain more realistic time-series (Perrault et al. 2013). Another advantage of this approach is that it is suitable for generating three component accelerograms, which could be required for non-linear dynamic analyses. Moreover the strong-motion duration of the natural accelerograms is conserved by the definition of the envelope. Two sets of natural accelerograms are chosen to provide the phases and envelopes:

- Natural accelerograms were selected from the French Accelerometric Network database (RAP, Péquegnat et al., 2008). We selected ten records corresponding to earthquakes with local magnitudes $M_L > 4$, focal depths less than 10 km, and that were recorded at epicentral distances shorter than 40 km, so that they present an acceptable signal-to-noise ratio. These ten accelerograms were then adjusted using the modified SIMQKE procedure. This is the fourth set of input motions and it is called here: *RAP_mSIMQKE*.

- The same process was performed but using the *Natural_Scaled* dataset instead, which presents a larger variability and matches the target spectrum better than does the RAP records. This is the fifth set of input motions and it is called here: *Natural_mSIMQKE*.

The semi-empirical non-stationary stochastic method previously developed by Pousse et al. (2006) and then improved by Laurendeau (2013) has the advantage of being both simple (it does not require detailed knowledge on the rupture, travel path or site conditions) and

accounting for basic concepts of seismology (Brune's source, a realistic envelope function, non-stationarity and variability). Time-domain simulations are derived from the signal spectrogram and depend on three strong-motion indicators (intensity measures): the relative significant duration (D_{SR}), the Arias intensity (AI) and the central frequency of the signal (FC(t)). For this study, the indicator distributions are deduced from the *Natural_Scaled* dataset. Many time histories are initially simulated (5 000) and scaled to the target PGA. Ten accelerograms are then randomly selected, and the distributions (μ and σ) of the key indicators (AI and D_{SR}) and the mean of the ten acceleration response spectra (SA) are computed. The procedure is repeated until: (1) the indicator distributions of the synthetics match those obtained from the *Natural_Scaled* dataset; and (2) the mean of the ten acceleration response spectra matches the target spectrum between 0.05 s and 2 s. To assess the goodness of fit, the formulation of Anderson (2004) was used for the five criteria and their sum was minimized. This leads to the sixth set of input motions and it is called here: *STOCH*. These ten accelerograms were then adjusted using the software SeismoMatch, in the period range 0.1 – 1s, which led to the seventh set of accelerograms: *STOCH_Matched.* For these two datasets, the match with the target spectrum is comparable to those of *Natural_Scaled* and *Natural_Matched*, with a lack of energy at short periods.

Table 2 presents the mean and variability of the three intensity measures considered when simulating the non-stationary stochastic accelerograms for the seven sets of time-series. We can observe that the *RAP_mSIMQKE* time-series have longer duration (D_{SR}) than the other ones, likely because the duration is fixed using records from distances up to 40 km. Figure 2 presents the accelerograms and spectra of these sets and as a measure of the variability in the spectra within each set, the coefficients of variation for spectral acceleration. From Table 2 and Figure 2 it can be seen that the *Natural_Scaled* set shows the greatest variability and the *SIMQKE* records the least. As expected, the calibrated stochastic

simulations (*STOCH* and *STOCH_Matched*) show variability close to that of the natural accelerograms (*Natural_Scaled* and *Natural_Matched*). It will be shown subsequently that this variability in input records carries over to variability in building and site response.

3. ANALYSIS OF BUILDING RESPONSE

In this section some analyses of building response using the seven sets of acceleration time-series are presented. We first conduct relatively simple structural modelling because of the number of runs that are required; but as shown below, the general trends carry over to more sophisticated dynamic analyses.

3.1. Analysis of Single Degree of Freedom (SDOF) systems

It is well known that structures do not remain elastic under strong shaking. To compare the effect of the seven sets of accelerograms presented above, we compute the nonlinear response of SDOF systems. The building behaviour is described following a model developed to simulate hysteretic energy capacity. In this paper, we used the Takeda model, first proposed by Takeda et al. (1970) and since analysed in depth by Schwab and Lestuzzi (2007) and Lestuzzi et al. (2007). The Takeda model includes realistic conditions for the reloading curves that model the characteristics of RC better than the standard elasto-plastic model. The Takeda model also accounts for the degradation of the stiffness with increasing excitation, which is related to the opening and closing process of existing cracks in the concrete, i.e. a reduction in the natural frequency of the building is accounted for. This behaviour is often observed in real structures under intense loading.

Five parameters are used to describe the Takeda model: the initial stiffness related to the natural frequency of the SDOF, the post-yield stiffness corresponding here to 5%, the coefficient α related to the stiffness degradation and the target β of the reloading curve. In this study, standard values are used to develop the Takeda model: $\alpha = 0.1$ and $\beta = 0.1$. The

strength reduction factor R is 2, corresponding to a structure having limited hysteretic energy dissipation capacity, and which is currently recommended by design codes. The last parameter is the yield displacement (U_y). Up to the yield point, the building capacity curve is assumed to be linear. U_y depends on the frequency of the structure (which generally correlates with its height) and different values are, therefore, considered.

For each set of accelerograms, three initial frequencies (periods) are considered: 1Hz (1s), 2Hz (0.5s) and 5Hz (0.2s) roughly corresponding to frequencies of low- and medium-rise RC buildings. For these frequencies, three U_y are chosen, according to the values provided in HAZUS (FEMA, 1999). We kept the values given for the C2 building class (i.e. concrete shear walls) and corresponding to the Low Code seismic standard: $U_y = 0.30$ cm for $f = 5$Hz, $U_y = 0.66$ cm for $f = 2$Hz and $U_y = 1.88$ cm for $f = 1$Hz. A damping ratio of 5% is used, which is a standard assumption for RC structures.

3.2. Results

Figure 3 shows the force-displacement of the Takeda-model for the Friuli record (#2, Table 1) and the 2Hz SDOF. We observe the hysteretic loops of the nonlinear behaviour of the system. The drift of the SDOF is also shown in Figure 3 (upper row), this parameter being chosen to compare the effect of the variability of the seismic ground motion in building response.

Considering the seven sets of accelerograms analysed in this paper, the three SDOF systems are tested and the drifts are compared (Figure 4 and Table 3). The building response shows large differences in terms of median and variability. The lowest variability is obtained for simulations using the *SIMQKE* method (sets 3, 4 and 5).The variability is the highest for the natural accelerograms (*Natural_Scaled*) and is well reproduced by the non-stationary stochastic simulations (*STOCH*). These two sets of accelerograms also result in similar median values. Finally, the median and the variability in the response at 2 Hz and 5 Hz using the natural matched (*Natural_Matched*) are similar to those obtained using the stochastic

matched (*STOCH_Matched*) (note, however, that for the 1 Hz SDOF system, the median and the variability using the *Natural_Matched* is larger). This is because the matching is performed in the frequency range 0.1 – 1 s, and one of the accelerograms is associated with high spectral accelerations above 1 s and hence high drifts at 1 Hz). This indicates that the natural variability of the ground-motion should be accounted for when selecting accelerograms and both methods integrating the natural or stochastic variability of ground motions are the most adapted. In addition, the overall variability of the drift increases for long-period buildings (1Hz). Depending on the features of the buildings, if this variability is neglected, the computed building response may underestimate the building response and the post-earthquake integrity of the building.

3.3. Analysis of a masonry building

To check the transferability of the results obtained for the simple SDOF system to masonry buildings, in this section we analyse the response of a sophisticated model of a masonry building developed by Gehl et al. (2013) to the same seven sets of accelerograms. Details of the analysed model and its calibration using an experimental pushover curve are provided in Gehl et al. (2013). Briefly, the model is of a simple two-storey brick building of size: 6m (length) × 4.4m (width) × 6.4m (height), with a computed natural period of 0.149s and higher modes (torsion and opposite-floor displacements) with periods around 0.05s. The model is subjected to the seven sets of accelerograms along its length using the TREMURI software, which discretizes the masonry into several components (piers, spandrels and rigid zones) through an equivalent-frame approach and macroelements.

Like for the analysis conducted on the simple ductile systems, the computed drifts for the masonry building and the seven sets of accelerograms show variable mean drifts and great differences between the observed variability around this mean (Figure 4). As with the ductile systems, the natural scaled accelerograms lead to the greatest variability and the

accelerograms generated using *SIMQKE* the least. The mean and the variability in the response using the *Natural_Matched* records is again similar to that observed using the stochastic records matched to the target spectrum (*STOCH_Matched*). This confirms the observation made above that the non-stationary stochastic approach of generating accelerograms proposed here is useful in capturing the true ground-motion variability and consequently the variability of building response.

4. ANALYSIS OF SOIL RESPONSE

Because nonlinear dynamic analyses are not only commonly conducted for building response but also for geotechnical studies, in this section the response of soil layers are analyzed using the same seven sets of accelerograms.

4.1. Method

The multi-shear mechanism model (Towhata and Ishihara, 1985) is a plane-strain formulation to simulate pore pressure generation in sands under cyclic loading and undrained conditions. Iai et al. (1990a, b) modified the model to account for the cyclic mobility and dilatancy of sands. The multiple-mechanism model relates the stress σ and strain ε through the following incremental equation (Iai et al., 1990a, b):

$$\{d\sigma'\} = [D](\{d\varepsilon\} - \{d\varepsilon_p\}) \quad (1)$$

where the curly brackets represent vector notation; $\{\varepsilon_p\}$ is the volumetric strain produced by the pore pressure, and [D] is the tangential stiffness matrix. This matrix is composed by the volumetric and shear mechanisms, which are represented by the bulk and tangential shear moduli, respectively. Each spring follows the hyperbolic stress-strain model (Konder and

Zelasko, 1963) and the generalized Masing rules for the hysteresis process (O'Connell et al., 2012). For more details on the model the reader is referred to Iai et al. (1990a, b).

Iai et al. (1995) thoroughly studied the soil response at Kushiro Port during the Kushiro-Oki M7.8 1993 earthquake. The soil column is composed of dense sands where the first 30 m are suspected of having strong dilatancy effects. In this paper, we use the same velocity model assumed to be overlaying EC8 site class B material with a shear wave velocity of 500 m/s so that it is consistent with the accelerograms chosen above. Furthermore, we keep Iai et al. (1995) dilatancy parameters to simulate pore pressure changes in the soil column in the first 30 m depth. As an input motion we use the 70 acceleration time-series presented in Section 2. The boundary condition at the bottom of the soil column is assumed to be an elastic boundary condition (outcrop ground motion). The incident wavefield is divided by two before computing wave propagation in order to remove the free-surface effect.

4.2. Results

The results of all computations are presented in terms of maximum shear deformation as a function of depth and response spectra of the resulting ground motion at the surface. Figure 5 (left) shows the geometric mean distribution of shear strain versus depth for each input set. Figure 5 (right) shows the coefficient of variation (C_V) for each dataset. These results indicate that, like building response, soil response is sensitive to the chosen acceleration time-series in spite of having the same response spectrum. The mean shear strain from 0 to 10 m depth is highest using the *RAP_mSIMQKE* set, likely because of their long durations. The large values of C_V for natural time-series indicate that natural variability should be taken into account when selecting spectrum-compatible accelerograms. In addition, this dispersion increases in layers where pore pressure effects take place. If this variability is neglected, the computed soil response may underestimate quite considerably the soil deformation.

Figure 6 shows the geometric mean response spectra (left) and the corresponding C_V

(right) for the time histories obtained at the surface for each dataset. These results are informative and show the complexity of ground-motion prediction when nonlinear soil behaviour takes place. Indeed, there is a partial correlation between the values of C_V and the resulting ground motion at the surface. For example, the natural data (black curve), which show the largest variability (C_V) do not lead to the highest response spectrum. This can be explained by looking at Figure 5 where the shear strain is largely mobilized by this dataset, thus strong nonlinearity occurs thereby reducing the computed ground motion at the surface. Conversely, the dataset having the smallest C_V (*SIMQKE*, yellow curve) has almost the largest response at the surface together with dataset from *Natural_mSIMQKE* in light blue. A special case is the one obtained using the non-stationary stochastic accelerograms because these records produce the strains closer to the natural signals and the C_V in terms of response spectra is also close to that dataset (red curve).

Finally, in spite of all these differences in terms of source generation and wave propagation, the resulting mean response spectra are relatively close. Nevertheless, these results suggest that care should be taken in selecting compatible time histories for soil response that includes nonlinear effects. It may not be sufficient to make only a few computations. It is probably a good idea to use several input ground motions to quantify the dispersion of the resulting ground motion at the surface.

5. CONCLUSIONS

This study shows that the selection of accelerograms is a fundamental component in earthquake engineering. Using various techniques we have generated seven sets of accelerograms following Eurocode 8 (EC8) guidance (i.e. with the constraint that their response spectra match the EC8 design spectrum) for a B site class, and analyzed their impact on nonlinear structures and soil columns. In both cases the mean, and especially the

variability of the nonlinear response depend greatly on the set of input accelerograms. It is thus crucial to select sets of accelerograms that represent the natural ground-motion variability. The small variability in the input set of accelerograms generated with the *SIMQKE* procedure and in the resulting structure response shows that a smaller number of accelerograms may be enough to determine the average structure behaviour but not necessarily the variability around this average.

Since the number of real accelerograms is sometimes limited for a given scenario, an alternative approach is to use non-stationary semi-empirical stochastic simulations (Laurendeau, 2013). This technique allows the rapid generation of many sets of realistic accelerograms with chosen variability of ground-motion parameters. Our results show that if the variability of the ground-motion indicators (Arias intensity and relative significant duration) are properly chosen (i.e. calibrated with real data), the stochastic method provides nonlinear responses of structures and soil columns (in terms of median value and variability) similar to those for natural accelerograms. For instance, the results presented in this paper could be expanded to site classes A and D using stochastic simulations with ground-motion indicators calibrated using the PEER database, which includes a large number of records for class B sites but fewer records for these site classes (site class C is well covered by natural accelerograms in the PEER database). Note, however, that such stochastic simulations are not suitable for generating three component accelerograms, which can be required for non-linear dynamic analyses. The approach that includes realistic phases in the original SIMQKE procedure (sets *RAP_mSIMQKE* and *Natural_mSIMQKE*) could represent an alternative method for this situation.

AKCNOWLEDGEMENTS

This work was partially sponsored by the Ministry of Sustainable Development through the French Accelerometric Network working group "Seismic ground motion for engineering". An earlier version was presented at the 15th World Conference on Earthquake Engineering (Lisbon, Portugal) in September 2012 (Laurendeau et al., 2012). We thank Pierre Gehl and Jaime Abad for computing the responses of the masonry structure and Pierino Lestuzzi for providing the Takeda code. We also thank Julien Rey for fruitful discussions. Finally, we thank two anonymous reviewers and Roberto Paolucci for their constructive comments on an earlier version of this article.

REFERENCES

Abrahamson, N. (1992). Non-stationary spectral matching, *Seismological Research Letters*, **63**(1), 30.

Abrahamson, N. A. and W. J. Silva (1996). Empirical ground motion models, *Report to Brookhaven National Laboratory*.

Anderson, J. (2004). Quantitative measure of the goodness-of-fit of synthetic seismograms, Proceedings of the 13th World Conference on Earthquake Engineering. Vancouver, Canada. Paper 243.

Atkinson, G. and K. Goda (2010). Inelastic seismic demand of real versus simulated ground-motion records for Cascadia subduction earthquakes, *Bulletin of the Seismological Society of America*, **100**(1), 102-115.

Bommer, J.J and A.B. Acevedo (2004). The use of real accelerograms as input to dynamic analyses, *Journal of Earthquake Engineering*, **8**, 43-91.

Boore, D. (2003). Simulation of ground motion using the stochastic method. *Pure and Applied Geophysics*, **160**(3):635–676.

Buratti, N., P. Stafford and J.J. Bommer (2011). Earthquake accelerogram selection and

scaling procedures for estimating the distribution of drift response, *Journal of Structural Engineering (ASCE)*, **137**, 345-357.

Douglas, J. (2006). Strong-motion records selection for structural testing. Proceedings of First European Conference on Earthquake Engineering and Seismology (a joint event of the 13th ECEE & 30th General Assembly of the ESC). Paper number 5.

Douglas, J. and H. Aochi (2008). A survey of techniques for predicting earthquake ground motions for engineering purposes, *Surveys in Geophysics*, **29**(3), 187-220. DOI 10.1007/s10712-008-9046-y.

Federal Emergency Management Agency (FEMA) (1999). HAZUS Earthquake loss estimation methodology. Federal Emergency Management Agency, Washington, D.C.

Gasparini, D. A. and E. H. Vanmarcke (1976). SIMQKE: A Program for Artificial Motion Generation, Department of Civil Engineering, Massachusetts Institute of Technology, Cambridge, MA.

Gehl, P., D. M. Seyedi and J. Douglas (2013). Vector-valued fragility functions for seismic risk evaluation, Bulletin of Earthquake Engineering, **11**(2), 365-384, DOI 10.1007/s10518-012-9402-7.

Giaralis, A. and P. D. Spanos (2009). Wavelet-based response spectrum compatible synthesis of accelerograms – Eurocode application (EC8), Soil Dynamics and Earthquake Engineering, **29**(1), 219-235.

Hancock, J., J. Watson-Lamprey, N. Abrahamson, J. Bommer, A. Markatis, E. McCoy and R. Mendis (2006). An improved method of matching response spectra of recorded earthquake ground motion using wavelets. *Journal of Earthquake Engineering*, **10(spec01)**:67–89.

Iai, S., Y. Matsunaga, and T. Kameoka (1990a). Strain space plasticity model for cyclic mobility, *Report of the Port and Harbour Research Institute*, **29**, 27-56.

Iai, S., Y. Matsunaga, and T. Kameoka (1990b). Parameter identification for cyclic mobility model, *Report of the Port and Harbour Research Institute*, **29**, 57-83.

Iai, S., T. Morita, T. Kameoka, Y. Matsunaga, and K. Abiko (1995). Response of a dense sand deposit during 1993 Kushiro-Oki Earthquake, *Soils and Foundations*, **35**, 115-131.

Iervolino, I., F. De Luca and E. Cosenza (2010a). Spectral shape-based assessment of SDOF nonlinear response to real, adjusted and artificial accelerograms, *Engineering Structures*, **32**, 2776-2792.

Iervolino, I., C. Galasso and E. Cosenza (2010b). REXEL: computer aided record selection for code-based seismic structural analysis. Bulletin of Earthquake Engineering, **8**, 339-362.

Kayhan, A.H., K. A. Korkmaz and A. Irfanoglu (2011). Selecting and scaling real ground motion records using harmony search algorithm, *Soil Dynamics and Structural Engineering*, **31**(7), 941-953.

Katsanos, E. I., A. G. Sextos and G. D. Manolis (2010). Selection of earthquake ground motion records: A state-of –the-art review from a structural engineering perspective, *Soil Dynamics and Structural Engineering*, 30, 157-169.

Konder, R.L. and J. S. Zelasko (1963). A hyperbolic stress-strain formulation for sands, in *Proceedings of Second Pan American Conference on Soil Mechanics and Foundation Engineering*, Brazil, 289-324.

Laurendeau, A. (2013). Définitions des mouvements sismiques au rocher. PhD thesis, Université de Grenoble.

Laurendeau, A., M. Causse, P. Guéguen, M. Perrault, L. F. Bonilla and J. Douglas, A set of Eurocode 8-compatible synthetic time-series as input to dynamic analysis, Proceedings of the Fifteenth World Conference on Earthquake Engineering. Lisbon, Portugal.

Lestuzzi, P., Y. Belmouden and M. Trueb (2007). Non-linear seismic behavior of structures

with limited hysteretic energey dissipation capacity, *Bulletin of Earthquake Engineering*, **5**(1), 549-569.

Motazedian, D. and G. M. Atkinson (2005). Stochastic finite-fault modeling based on a dynamic corner frequency, *Bulletin of the Seismological Society of America*, **95**, 995–1010

O'Connell, D., J. P. Ake, L. F. Bonilla, P. Liu, R. LaForge, and D. Ostenaa (2012). Strong ground motion estimation, in *Earthquake Research and Analysis – New Frontiers in Seismology*, ISBN 978-953-307-840-3.

Özer, B. and S. Akkar (2012). A procedure on ground motion selection and scaling for nonlinear response of simple structural systems, *Earthquake Engineering and Structural Dynamics*, **41**(12), 1693-1707. DOI: 10.1002/eqe.1198.

Pequegnat C., Gueguen P., Hatzfeld D., Langlais M. 2008. The French Accelerometric Network (RAP) and National Data Centre (RAP-NDC). *Seismological Research Letters*, **79**(1), 79-89.

Perrault, M., P. Guéguen, A. Aldea and S. Demetriu (2013). Reducing the uncertainties of the fragility curves using experimental testing in existing buildings: the case of the BRD Tower of Bucharest (Romania), *Earthquake Engineering and Engineering Vibration*, in press.

Pousse, G., C. Berge-Thierry, F. Bonilla and P.Y. Bard (2005). Eurocode 8 design response spectra evaluation using the K-Net Japaneese database, *Journal of Earthquake Engineering*, **9**, 547-574.

Pousse, G., L. F. Bonilla, F. Cotton, L. Margerin (2006). Nonstationary stochastic simulation of strong ground motion time histories including natural variability: Application to the K-net Japanese database. *Bulletin of the Seismological Society of America*, **96**, 2103–2117.

Rezaeian, S. and A. Der Kiureghian (2010). Simulation of synthetic ground motions for

specified earthquake and site characteristics. *Earthquake Engineering & Structural Dynamics,* **39**, 1155–1180.

Rota, M., E. Zuccolo, I. Taverna, M. Corigliano, C. G. Lai and A. Penna (2012). Mesozonation of the Italian territory for the definition of real spectrum-compatible accelerograms, *Bulletin of Earthquake Engineering*, **10**(5), 1357-1375. DOI 10.1007/s10518-012-9369-4.

Sabetta, F. and A. Pugliese (1996). Estimation of response spectra and simulation of nonstationary earthquake ground motions, *Bulletin of the Seismological Society of America*, **86**, 337-352.

Schwab, P. and P. Lestuzzi (2007). Assessment of the seismic non-linear behavior of ductile wall structures due to synthetics earthquakes, *Bulletin of Earthquake Engineeering,* **5**, 67-84.

Sextos, A. G., E. I. Katsanos and G. D. Manolis (2011). EC8-based earthquake record selection procedure evaluation: Validation study on observed damage of an irregular R/C building, *Soil Dynamics and Structural Engineering,* **31**, 583-597.

Silva, W. and Lee, K. (1987). WES RASCAL code for synthesizing earthquake ground motions: State-of-the-Art for Assessing Earthquake Hazards in the United States, Report 24. *US Army Engineers Waterways Experiment Station, Misc. Paper S-73-1*.

Takeda, T., M. A. Sozen and N. M. Nielsen (1970). Reinforced concrete response to simulated earthquakes, *Journal of the Structural Division,* **96**(ST12), 2557-2573. Proceedings of the American Societey of Civil Engineers (ASCE).

Towhata, I. and K. Ishihara (1985). Modeling soil behavior under principal axes rotation, paper presented at the *Fifth International Conference on Numerical Methods in Geomechanics*, Nagoya, Japan, 523-530.

Watson-Lamprey, J. and N. Abrahamson (2006). Selection of ground-motion time series and

limits on scaling, *Soil Dynamics and Structural Engineering*, **26**, 477-482.

Tables

Table 1. *Natural_Scaled* dataset.

	Event	M_w	Station	Component (°)	r_{rup} (km)	V_{s30} (m/s)	Unscaled PGA (g)
1	Parkfield	6.19	Temblor pre-1969	295	16.0	528	0.27
2	Friuli, Italy-02	5.91	Forgaria Cornino	270	14.8	412	0.21
3	Irpinia, Italy-02	6.20	Calitri	270	8.8	600	0.17
4	Morgan Hill	6.19	Anderson Dam (Downstream)	250	3.3	488	0.42
5	San Salvador	5.80	Geotech Investig Center	90	6.3	545	0.87
6	Whittier Narrows-01	5.99	Garvey Res, - Control Bldg	330	14.5	468	0.46
7	Northridge-04	5.93	Moorpark - Fire Sta	180	14.7	405	0.18
8	Chi-Chi, Taiwan-02	5.90	TCU073	0	10.7	508	0.09
9	Chi-Chi, Taiwan-03	6.20	TCU078	0	7.6	443	0.28
10	Chi-Chi, Taiwan-04	6.20	CHY074	90	6.2	553	0.32
Mean M_w		6.05	Mean r_{rup}, V_{s30} and unscaled PGA		10.3	495	0.33

M_w is moment magnitude, r_{rup} is distance to the rupture and V_{s30} is the average shear-wave velocity in the top 30m. The horizontal component used is expressed in term of azimuth. Note that in the event column, 01 corresponds to the mainshock and 02,03,... to aftershocks.

Table 2: Mean and variability of three key intensity measures for the seven sets of records.

		Ln(PGA)		Ln(AI)		Ln(D_{SR})	
		Exp(μ) (m/s^2)	Exp(σ) (m/s^2)	Exp(μ) (m/s)	Exp(σ) (m/s)	Exp(μ) (s)	Exp(σ) (s)
1	Natural_Scaled	2.16	1.00	0.33	1.80	7.24	1.74
2	Natural_Matched	2.23	1.16	0.29	1.51	7.66	1.63
3	SIMQKE	2.20	1.00	0.69	1.20	7.65	1.02
4	RAP_mSIMQKE	2.36	1.06	0.90	1.22	16.41	1.29
5	Natural_mSIMQKE	2.53	1.14	0.51	1.28	8.74	1.38
6	STOCH	2.16	1.00	0.35	1.82	7.23	1.71
7	STOCH_Matched	2.12	1.13	0.34	1.61	7.45	1.82

PGA is peak ground acceleration, AI is Arias intensity and D_{SR} is relative significant duration equal to the time interval between 5% and 95% of the cumulative AI over time.

Table 3: Comparison of the mean and variability of the drift computed for SDOF systems (RC buildings) at 1 Hz, 2 Hz and 5 Hz, and the masonry building, for the seven sets of accelerograms.

		SDOF system – 1 Hz		SDOF system – 2 Hz		SDOF system – 5 Hz		Masonry building	
		median	std	median	std	median	std	median	std
1	Natural_Scaled	0.140	0.120	0.157	0.118	0.090	0.032	0.368	0.140
2	Natural_Matched	0.099	0.015	0.111	0.034	0.095	0.021	0.341	0.077
3	SIMQKE	0.099	0.020	0.102	0.015	0.089	0.006	0.316	0.035
4	RAP_mSIMQKE	0.118	0.013	0.112	0.017	0.082	0.007	0.417	0.067
5	Natural_mSIMQKE	0.103	0.016	0.100	0.019	0.084	0.009	0.293	0.032
6	STOCH	0.175	0.104	0.181	0.070	0.091	0.028	0.412	0.162
7	STOCH_Matched	0.161	0.094	0.115	0.018	0.094	0.012	0.355	0.077

Figure captions

Figure 1. Comparison between the standard EC8 spectra and the spectra applied in France (Type 1 and 2), for a type B site. For periods below 1s the French Type 2 spectrum is the same as the standard EC8 spectrum and hence it is plotted beneath this curve.

Figure 2. Left: The seven sets of accelerograms generated for the nonlinear dynamic analyses. The PGA values are all equal to ~2.2 m/s^2. Middle: Corresponding response spectra (gray), geometric mean of response spectra (black) and EC8 design spectrum for type B soil (red). Right: Coefficient of variation of spectral acceleration.

Figure 3. Example of drift (left, upper figure) and force-displacement curve (right), for the 2Hz SDOF building using the Friuli record (#2, Table 1; left, lower figure).

Figure 4. Comparison of the drifts computed for SDOF systems at 1Hz (grey circles), 2Hz (black circles), 5Hz (open circles) and masonry (grey squares) buildings, for the seven sets of accelerograms. For the sets *Natural_Scaled* and *STOCH*, median and standard deviation (represented by red dashes) are computed by removing the drift values larger than 0.8.

Figure 5. Distribution of maximum shear deformation versus depth (left). Each line corresponds to the geometric mean strain of each dataset (Table 2). Coefficient of variation versus depth for each computed dataset (right).

Figure 6. Mean response spectra of computed ground motion at the surface (left) and the corresponding coefficient of variation (right).

Figures

Figure 1

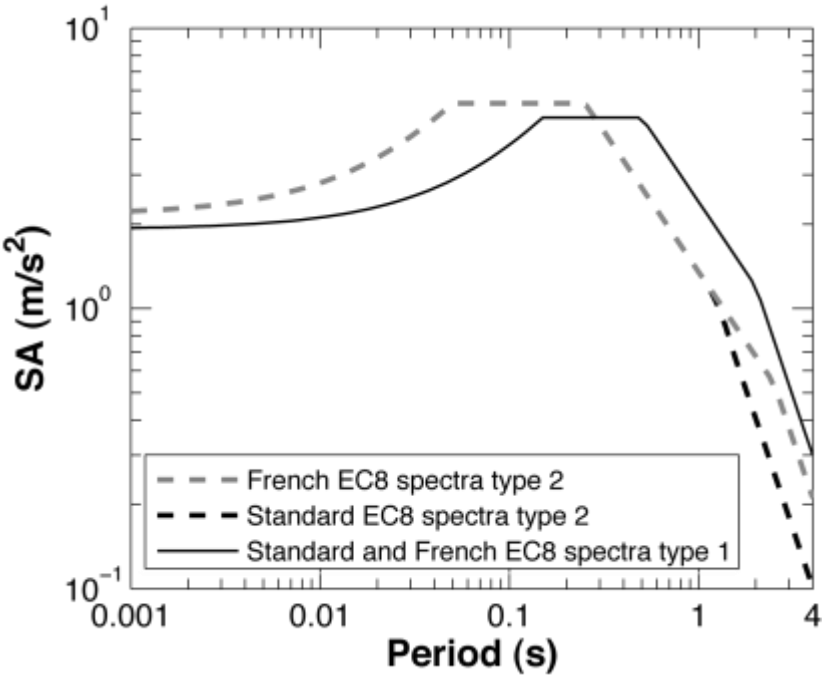


Figure 2

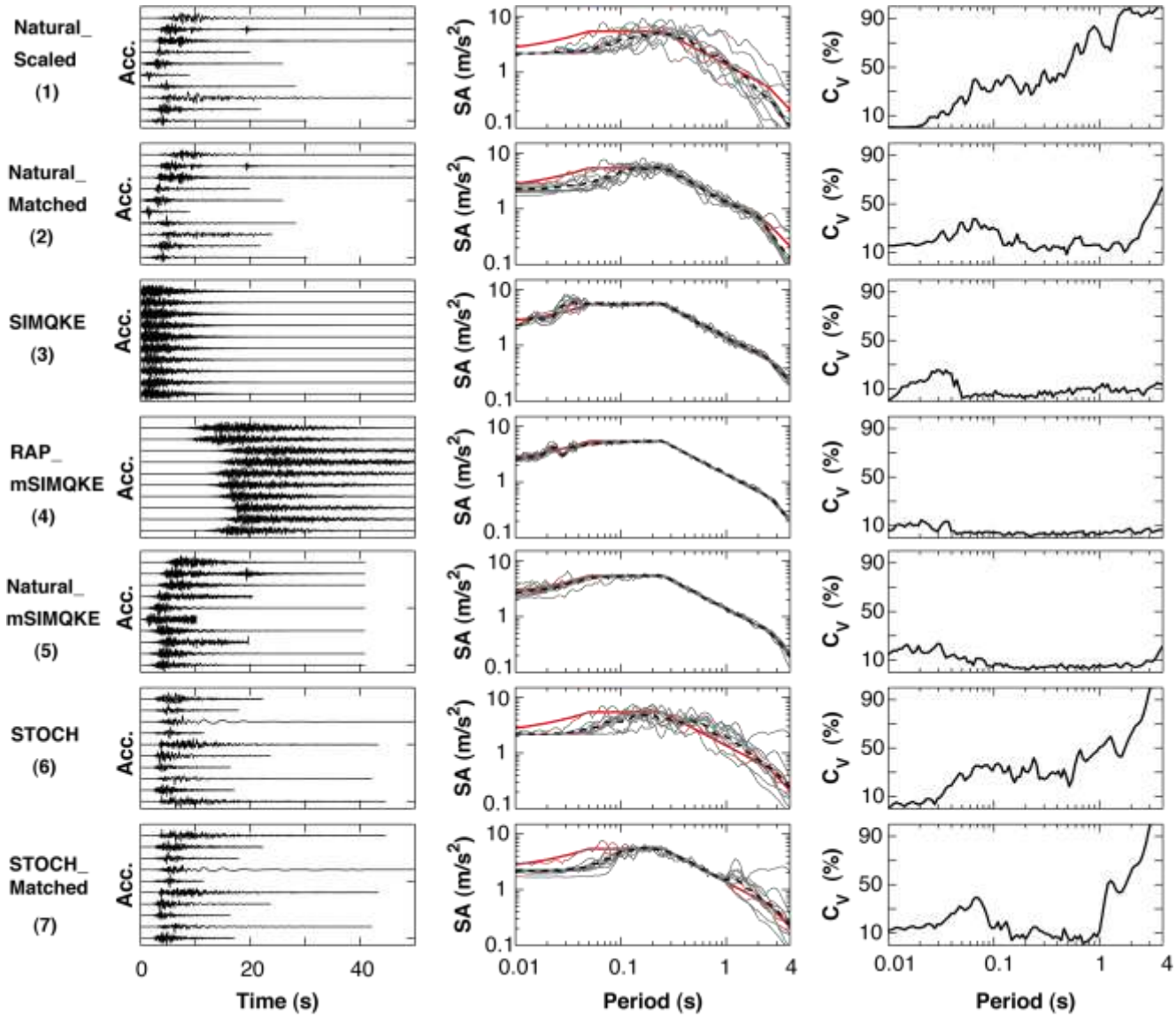

Natural_
Scaled
(1)
Natural_
Matched
(2)
SIMQKE
(3)
RAP_
mSIMQKE
(4)
Natural_
mSIMQKE
(5)
STOCH
(6)
STOCH_
Matched
(7)
Acc.
SA (m/s²)
C_V (%)
0
20
40
Time (s)
0.01
0.1
1
4
Period (s)
10
1
0.1
90
50
10

Figure 3

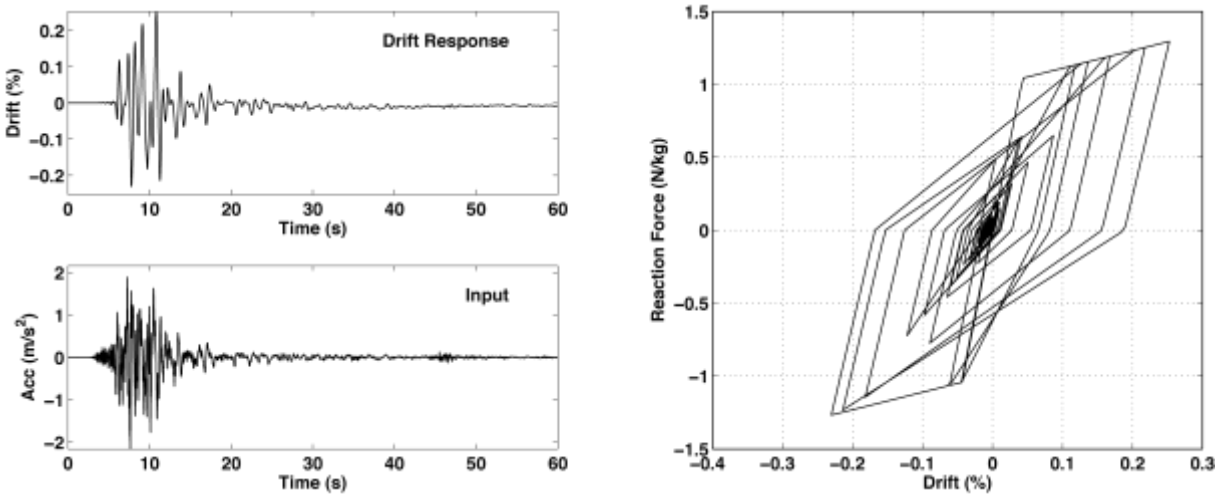

Drift Response
Drift (%)
Time (s)
Input
Acc (m/s²)
Time (s)
Reaction Force (N/kg)
Drift (%)

Figure 4

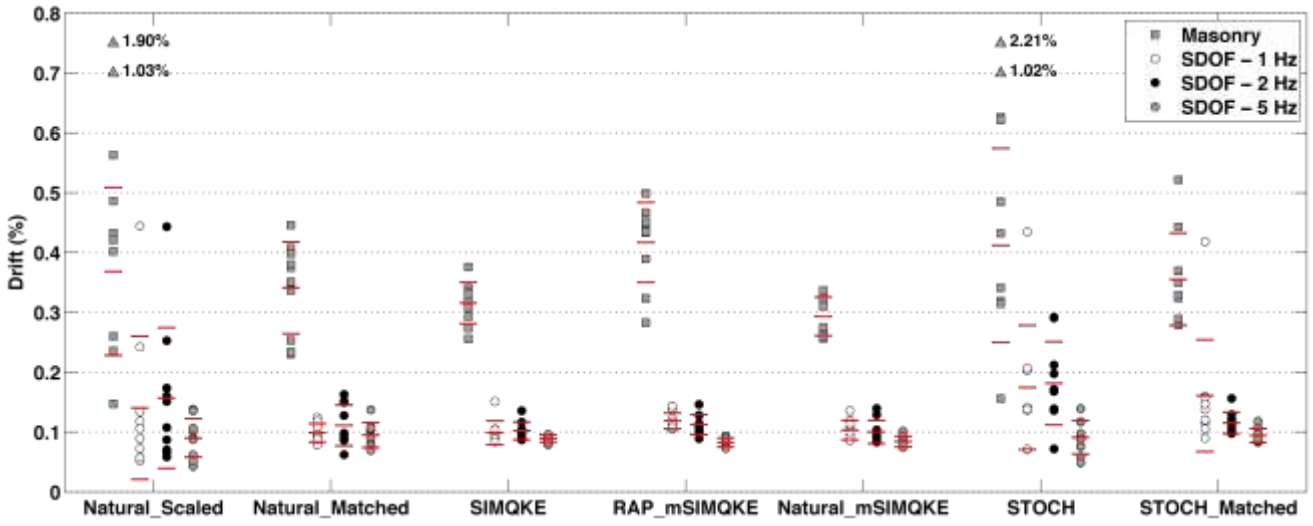

Drift (%)
0.8
0.7
0.6
0.5
0.4
0.3
0.2
0.1
0
1.90%
1.03%
2.21%
1.02%
Masonry
SDOF – 1 Hz
SDOF – 2 Hz
SDOF – 5 Hz
Natural_Scaled
Natural_Matched
SIMQKE
RAP_mSIMQKE
Natural_mSIMQKE
STOCH
STOCH_Matched

Figure 5

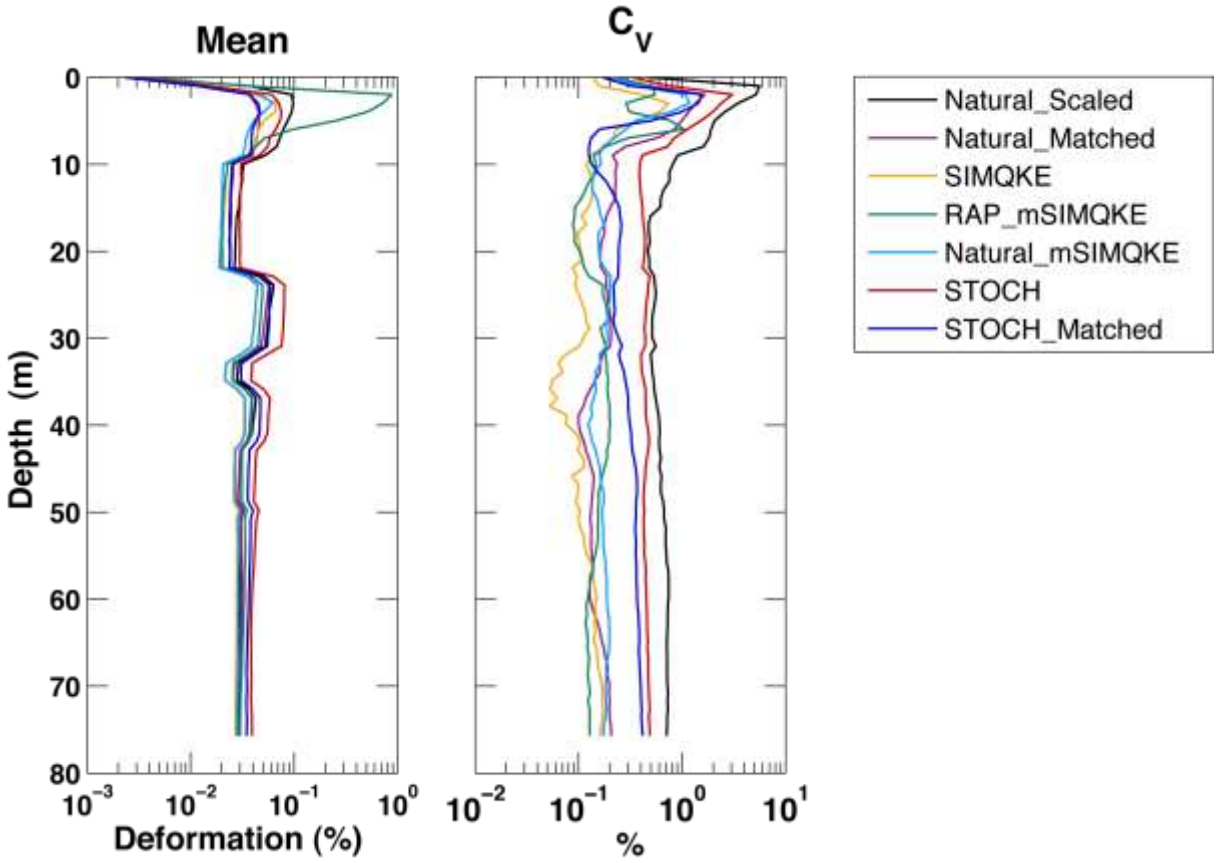
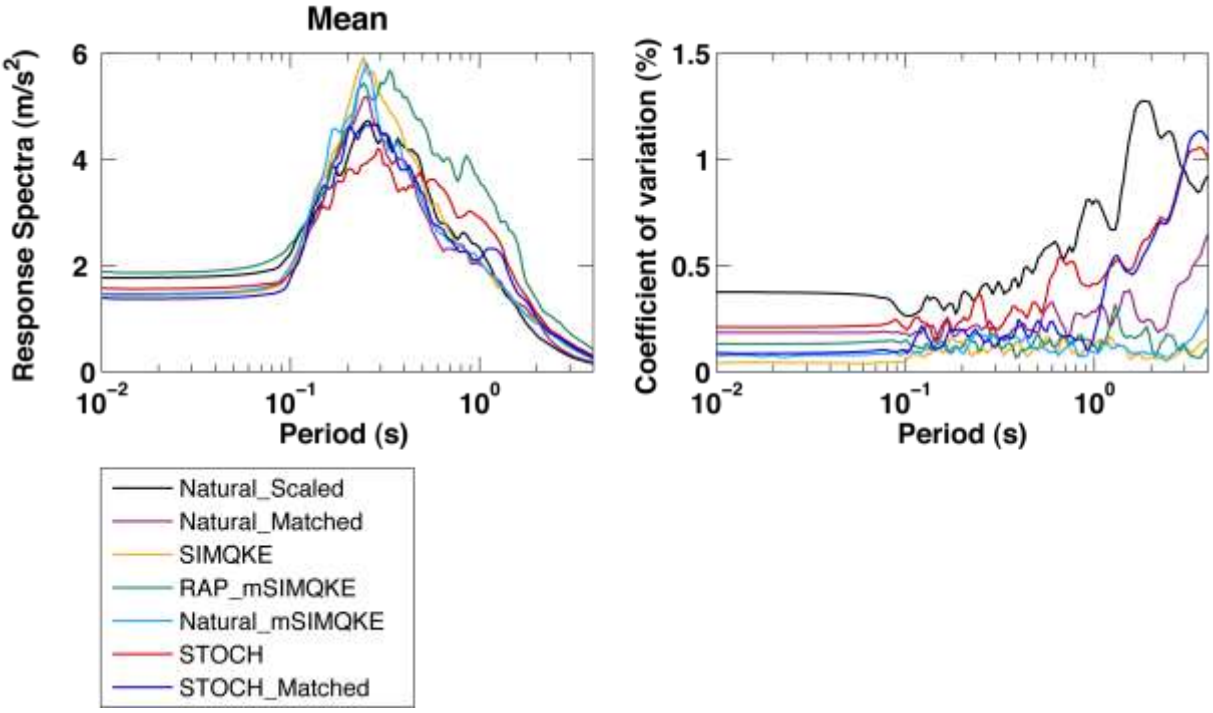

Mean
C_v
Depth (m)
0
10
20
30
40
50
60
70
80
10^{-3}
10^{-2}
10^{-1}
10^{0}
Deformation (%)
10^{-2}
10^{-1}
10^{0}
10^{1}
%
Natural_Scaled
Natural_Matched
SIMQKE
RAP_mSIMQKE
Natural_mSIMQKE
STOCH
STOCH_Matched

Figure 6


Mean
Response Spectra (m/s²)
Period (s)
Coefficient of variation (%)
Period (s)
Natural_Scaled
Natural_Matched
SIMQKE
RAP_mSIMQKE
Natural_mSIMQKE
STOCH
STOCH_Matched